Journal of
Ceramic Science
and Technology

J. Ceram. Sci. Tech., 02 [01] 31-38 (2011)
DOI: 10.4416/JCST2010-00023
available online at: http://www.ceramic-science.com
© 2011 Göller Verlag

Nanoscopic Metal Fluorides as Promising Sintering Aids for High-Performance Alumina Ceramics

Ch. Stosiek[1], H. Ludwig[2], U. Reichel[2], G. Scholz[1], E. Kemnitz[*1],

[1]Department of Chemistry, Humboldt University of Berlin, Brook Taylor Strasse 2, Germany 12489 Berlin
[2]Fraunhofer Institute for Ceramic Technologies and Systems, Institutsteil Hermsdorf,
Michael-Faraday-Str. 1, Germany 07629 Hermsdorf

received June 18, 2010; received in revised form August 18, 2010; accepted September 24, 2010

Abstract

Nanoscopic aluminium fluoride and magnesium fluoride were investigated as sintering additives for high-purity alumina ceramic production.

Nanoscopic magnesium fluoride has been found to be an excellent sintering additive. It enables an effective limitation of grain growth compared to standard ceramic production, thus resulting in ceramics with high density, sub-µm grain size and low concentration of defects, which are perfect preconditions for an improvement of mechanical strength, transparency as well as optical properties. As a result, transparent corundum ceramics with a Vickers hardness of about 3200 were obtained. A mechanistic interpretation of the possible chemical role of nano-MgF_2 in the course of texture formation, crystal growth, and densification of the corundum particles is presented based on DTA-TG and ^{19}F MAS NMR-investigations.

However, in contrast to literature reports, AlF_3 is not suitable for the preparation of slurries and spray granulates with application of the standard technology mainly due to
i) its extreme Lewis acidity,
ii) phase transformation and sublimation starting at around 700 °C, and
its strong tendency toward pyrohydrolysis, resulting altogether in outgassing effects.

Keywords: Transparent, hard alumina ceramic, nano magnesium fluoride, nano aluminium fluoride,mechanical strength, sintering additive

I. Introduction

The development of stronger, more versatile ceramics for advanced technological applications, such as engines, electronic components, catalysts, superconductors, or sensors, is one of the main challenges of materials scientists. Among the diversity of ceramic materials, oxide ceramics, and especially corundum ceramics, occupy an outstanding position on account of their excellent properties. Applications in medical engineering (e.g. in endoprosthesis), in environmental technologies (e.g. as filtration membranes), or as pressure sensors are now well known [1,2]. More recently, the use of corundum ceramics with high transparency for optical applications has been described [3,4]. Such high-performance materials require properties like high mechanical strength, toughness and hardness, high corrosion resistance, and purity. Considerable advantages concerning such properties would arise from advantages in fine grain structure, in a more homogeneous and defect-free structure and high purity of Al_2O_3 [5, 6]. Usually, the doping of alumina for minimizing grain growth entails adding oxides in low amounts (usually less than 1 %) [7,8].

So far, transparent corundum ceramics have been doped with 0.1 % MgO. Nevertheless, a sintering temperature of more than 1350 °C is necessary during ceramic processing to obtain such high-purity and high-density alumina ceramics based on commercially available powders.

Interestingly, from the literature it is well known that the use of oxides in combination with metal fluorides as additives (0.05 % up to 2.5 %) can improve the microstructure and properties of ceramics as a consequence of the reduced sintering temperature [9,10]. A small grain size of the additive is necessary and the particles have to be finely dispersed within the oxide matrix. Usually, the first point, a small particle size of the fluorides, can be achieved by milling of crystalline fluorides [11,12]. With the ball mills mainly accessible for technical purposes, however, final grain sizes are restricted to the range of 100 nm or more. The second important point, the fine and homogeneous dispersion of milled fluorides in the oxide matrix, requires extensive experience in ceramic processing.

Both limiting pre-conditions can be overcome by using the fluorolytic sol-gel synthesis for the preparation of nanoscopic metal fluorides developed by Kemnitz *et al.* in 2003 [13,14]. Stable liquid sols or dry nanoscopic, X-ray amorphous metal fluoride powders with high surface areas can be obtained after the solvent is removed. With a

* Corresponding author: erhard.kemnitz@chemie.hu-berlin.de

comparably uniform particle size distribution in the range of only few nanometres these fluorides are predestined for use as sintering aids. They offer the general possibility to produce high-purity Al_2O_3 ceramics with microstructures in the sub-μm range and nanoscaled doping.

Therefore it is the intention of the present study to test the ability of dry nanoscopic metal fluorides prepared based on the sol-gel route for the formation of corundum ceramics with improved optical properties and mechanical strength. This is ultimately only possible if doping with these fluorides helps to reduce the sintering temperature and consequently to restrict grain growth and homogenize the microstructure.

Two nanoscopic metal fluorides were chosen for the present study: AlF_3 and MgF_2. Owing to the crystallization of a-AlF_3 and a-Al_2O_3 within the same space group in line with previously published studies, AlF_3 was expected to be the most suitable additive for the corundum [15,16]. For comparative purposes, also with MgO as additive, nanoscopic MgF_2 was used in our study.

II. Experimental

(1) Preparation of fluoride samples

The metal fluorides were prepared with the sol-gel method using Schlenk techniques in an argon atmosphere because all the precursor compounds are moisture-sensitive and the products all tend to adsorb water. Methanol (MeOH) was dried over Mg and distilled prior to use. Tetrahydrofurane (THF) was dried over Na and distilled prior to use. Aluminium isopropoxide, magnesium metal and hydrofluoric acid (50 wt%) were purchased from Aldrich. The procedure for the preparation of aluminium fluoride is as follows: [16] aluminium isopropoxide (6.6 g, 32 mmol) was dissolved in 100 ml dry THF to avoid uncontrolled hydrolysation, and hydrofluoric acid (3.3 ml, 96 mmol) was slowly added in a molar ratio of Al : F = 1 : 3 under stirring at room temperature. The resulting sol was stirred for 20 min followed by the removal of the solvent and formed isopropanol under reduced pressure; the white powder finally obtained was dried at 180 °C under vacuum.

For the preparation of magnesium fluoride, magnesium metal (0.8 g, 32 mmol) was treated with 50 ml dry methanol overnight at room temperature. To the formed $Mg(OMe)_2$ solution, hydrofluoric acid (2.3 ml, 64 mmol) was slowly added (molar ratio of Mg : F = 1 : 2) under stirring at room temperature. The resulting sol was stirred for 20 min followed by the removal of the solvent under reduced pressure. The white powder finally obtained was dried at 180 °C under vacuum.

(2) Characterization of fluoride materials

For X-ray powder diffraction measurements, Seiffert XRD 3003 TT equipment (Freiberg, Germany) with Cu*K*α radiation was applied. Phases were identified by comparison with the ICSD powder diffraction file [17].

MAS NMR spectra were recorded at spinning speeds of 20, 25, or 30 kHz and a resonance frequency of 376.4 MHz for ^{19}F on a Bruker AVANCE 400 spectrometer equipped with a 2.5 mm MAS probe.

^{19}F MAS NMR *(I = 1/2)* spectra were recorded with a π/2 pulse duration of $p1 = 2$ μs, a spectrum width of 400 kHz, a recycling delay of 10 s, and an accumulation number of 64. Isotropic chemical shifts of ^{19}F are given with respect to the $CFCl_3$ standard. Background signals of ^{19}F could be completely suppressed with the application of a phase-cycled depth pulse sequence according to Cory and Ritchey [18].

Elemental analyses of the samples were performed with LECO CHNS-932 combustion equipment (C, H, N). The fluoride contents were determined with a fluoride-sensitive electrode after conversion of the solids with Na_2CO_3/K_2CO_3 into a soluble form. The aluminium and magnesium contents of the samples were determined by ICP OES (IRIS Intrepid HR DUO) after a microwave-assisted (ETHOS plus) conversion with a H_3PO_4/HNO_3-mixture into a soluble form. The instrument was calibrated with standard solution.

Thermal analysis experiments were performed on a STA 409 C (Netzsch Gerätebau GmbH, Selb, Germany) equipped with a Balzers QMG 422 quadrupole mass spectrometer. A DTA-TG sample-holder system (Pt/PtRh10 thermocouple) was used. Measurements were performed in a N_2 atmosphere.

Particle sizes of the samples were determined with an Ultrafine Particle Analyser (Microtrac). To prevent agglomeration, the suspension (sample in water) was sonicated prior to the measurement. The particle size distribution was determined with laser light of a wavelength of 780 nm.

The surface areas of the samples were determined using Ar absorption by means of an ASAP 2020 instrument (Micromeritics) at 77 K. Before each measurement, the samples were degassed at $5 \cdot 10^{-5}$ mbar and 150 °C for 12 h. The isotherms were processed based on Brunauer-Emmett-Teller (BET) models.

Electrochemical streaming potentials and pH-values were determined with a PCD-Particle Charge Detector (MÜTEK PCD 03 pH).

(3) Preparation of ceramic samples

A commercially available high-purity corundum powder was used as starting material, supplied by Taimicron TM-DAR (Taimei Chemicals Co.Ltd.) with the certification as follows: purity > 99.99 %; specific surface area (BET): 14 m^2/g; particle size $d_{50} = 0.15$ μm.

The ceramic samples for final characterization were produced according to the following procedure:

First, slurries were manufactured by milling and dispersing the alumina powder in water containing a dispersant (CE 64, Zschimmer & Schwarz, Lahnstein). Then, the respective metal fluorides were added as dopants in the form of nano-powders with nominal quantities ranging from 0.05 up to 2 wt% in a Minicer laboratory agitator bead mill (Netzsch). All grinding chamber parts of the Minicer consist of wear-resistant zirconium oxide, the size of grinding balls being 500 μm. In a second step, slip casting was performed in a plaster mould for drying the samples. And in a third step, sintering in air under different heating conditions (temperature range from 1280 °C to 1340 °C) followed by partly hot isostatic pressing (HIP, temperature range from 1280 °C to 1350 °C) was performed.

The as-prepared samples were used for the characterization of the materials properties: sintered density (hydrostatic weighing), sintered structure (crystal size, porosity, inhomogeneities) by SEM on polished and thermally etched probes, including image evaluation to determine the particle size distribution; Vickers hardness HV0,1 (Vickers Microhardness in accordance with DIN/ISO 4516); transmission on ground and polished discs in a spectral range from λ = 300 – 2200 nm, measured with Carl Zeiss MicroImaging apparatus (light path length 50 mm determined at 8°; ^{19}F MAS NMR spectroscopic investigation of the reaction path of MgF_2-dopant).

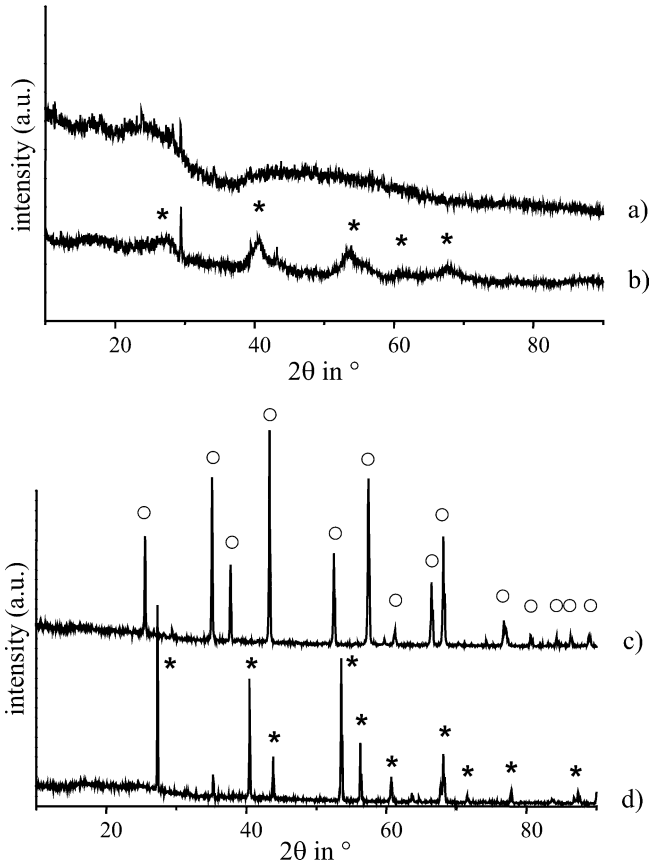

Fig. 1: X-ray diffractograms of (a) AlF_3 and (b) MgF_2 after drying at 180 °C as well as (c) AlF_3 and (d) MgF_2 after thermal annealing at 900 °C in air (heating rate 20 °C/min, 4 h dwell time). *: reflections of MgF_2; ○: reflections of Al_2O_3.

III. Results

(1) Synthesis, characterization and thermal behaviour of the pure fluoride phases

The synthesis of various metal fluorides via a sol-gel route using *anhydrous* HF in organic solvents was first developed in our group [13, 19]. These reactions lead to X-ray amorphous metal alkoxide fluorides with very high specific surface areas. Following the reaction equations:

$$Al(O^iPr)_3 + 3HF_{(aq.)} \rightarrow AlF_3 + 3^iPrOH \quad (1),$$

or

$$Mg(OMe)_2 + 2HF_{(aq.)} \rightarrow MgF_2 + 2MeOH \quad (2),$$

respectively, the sol-gel synthesis of metal fluorides using *aqueous* HF solution leads to X-ray amorphous, nanoscopic compounds with high *Lewis*-acidity (AlF_3) or medium *Lewis*– and *Brønstedt*-acidity (MgF_2), respectively [13, 14, 20]. The particle sizes of the metal fluorides (d_{95}-values), determined by dynamic light scattering, were 4.7 nm (AlF_3) or 8.3 nm (MgF_2), respectively. In Fig. 1, the X-ray diffractograms of AlF_3 (Fig. 1, a) and MgF_2 (Fig. 1, b) after drying at 180 °C are shown. In the XRD pattern of AlF_3, no reflections are visible, whereas the diffractogram of MgF_2 shows at least three very broad reflections, assignable to MgF_2. The absence of distinct reflections is a clear argument for the high degree of disorder in the structures of the samples. In Table 1, the elemental compositions, BET surface areas, porosity types, average pore diameters, and particle sizes of the synthesized samples are summarized. In comparison to the crystalline metal fluorides, the surface areas of the nanoscopic compounds are extremely high. This can be attributed to the high degree of structural disturbance of the phases, caused by the sol-gel synthesis. In Fig. 2, the ^{19}F MAS NMR spectra of AlF_3 and MgF_2 after drying at 180 °C are shown. The ^{19}F MAS NMR spectrum of nanoscopic AlF_3 consists of three signals (Fig. 2, a). The central signal at -165 ppm is typical for the presence of $AlF_x(OH)_{6-x}$-octahedra with $x \geq 5$ as mean coordination in AlF_3 [16, 21, 22]. The asymmetry and the broadness of the central line is caused by the superimposition of signals of different $AlF_x(OH)_{6-x}$-octahedra with a distribution of Al-F-bond lengths and -angles. The peak at -123 ppm is caused by (possibly) adsorbed HF [23, 24], whereas the signal at -190 ppm shows the existence of terminal F sites, which confirm the high degree of structural disturbance of the sample [16, 25, 26]. The ^{19}F spectrum of nanoscopic MgF_2 (Fig. 2, b) consists of one single peak at -198 ppm, at typical value for MgF_6-octahedra in MgF_2.[27] Also, this signal is relatively broad and asymmetric, owing to the structural disorder of the sample.

Table 1: Elemental composition, BET surface area, porosity type, average pore diameter and mean particle size of synthesised samples.

	AlF_3	MgF_2
Al	26.0 wt %	—
Mg	—	37.5 wt%
F	54.7 wt %	57.2 wt %
M/F	$1 : 2.9_9$	$1 : 1.9_2$
H	2 wt%	b.d.
average composition	$AlF_3 \cdot 1.1H_2O$	$MgF_{1.95}(OH)_{0.05}$
surface area	130 m²/g	232 m²/g
porosity type	meso porous	meso porous
average pore diameter	79Å	33Å
mean particle size (d_{50})	4.1 nm	6.1 nm

M/F: molar ratio of metal (Al or Mg) and F, b.d.: below detection limit.

The thermoanalytic plots (DTA) of AlF_3 (Fig. 3, a) and MgF_2 (Fig. 3, b) show the different thermal behaviour of the both different metal fluorides. The thermal decomposition of AlF_3 occurs in two steps (TG curve). The mass loss of 19.9 % (calc.: 19.4 %) corresponds to water release

from the sample ($AlF_3 \cdot 1.1H_2O \rightarrow AlF_3 + 1.1H_2O \uparrow$). The difference between the measured and calculated values is explainable by the generation of HF and $HAlF_4$ as a result of partial pyrohydrolysis of the samples caused by the released water of the sample itself. The simultaneous release of H_2O, HF, and $HAlF_4$ occurs exactly in the temperature region described by Menz *et al.* [28]. The second step of the thermal decomposition of AlF_3 is caused by sublimation and pyrohydrolysis of AlF_3 resulting in Al_2O_3 according to Eq. (3):

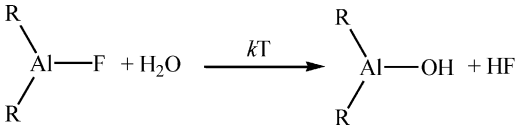

(3)

The pyrohydrolysis is confirmed by XRD and the X-ray diffraction pattern of AlF_3 shows, after thermal annealing at 900 °C in air, reflections of corundum as the only phase (Fig. 1, c). Also the ^{19}F NMR spectrum of AlF_3 depicts the loss of fluorine, the resulting signal of the annealed sample has a worse signal-to-noise ratio and is less intensive (Fig. 2, c).

The thermal behaviour of nanoscopic MgF_2 is completely different. The DTA shows only a low mass loss, caused by the release of (surface-bonded) water (Fig. 3, b). Between 300 °C and 1250 °C, nanoscopic MgF_2 is stable, no decomposition but only grain growth and crystallization of the MgF_2 occur. This finding is supported by XRD (Fig. 1, d), where only reflections of crystalline MgF_2 are detectable, and by ^{19}F MAS NMR (Fig.2, d). Here the typical signal of MgF_6-octahedra in MgF_2 at -198 ppm is visible. Because of the crystallization, the line width of the signal is narrow and there is no asymmetry left.

Because it was anticipated that nanoscopic sintering additive materials might have a special impact arising from their nanoscopic nature, the rheological properties of these new materials have been investigated in more detail. The particle size distributions of the pure fluoride phases determined by the laser diffraction method are shown in Figs. 4a (AlF_3) and 4b (MgF_2). As can be seen, both samples consist of very small nano-particles and exhibit narrow particle size distributions.

The electrochemical streaming potentials (PCD) of the nanoscopic fluorides in comparison to pure alumina and post-fluorinated AlF_3 (AlF_3-F) are presented in Fig. 5. There are big differences in the pH-values at the isoelectric points (point of zero charge) between AlF_3 and MgF_2 with extremely acidic properties of AlF_3.

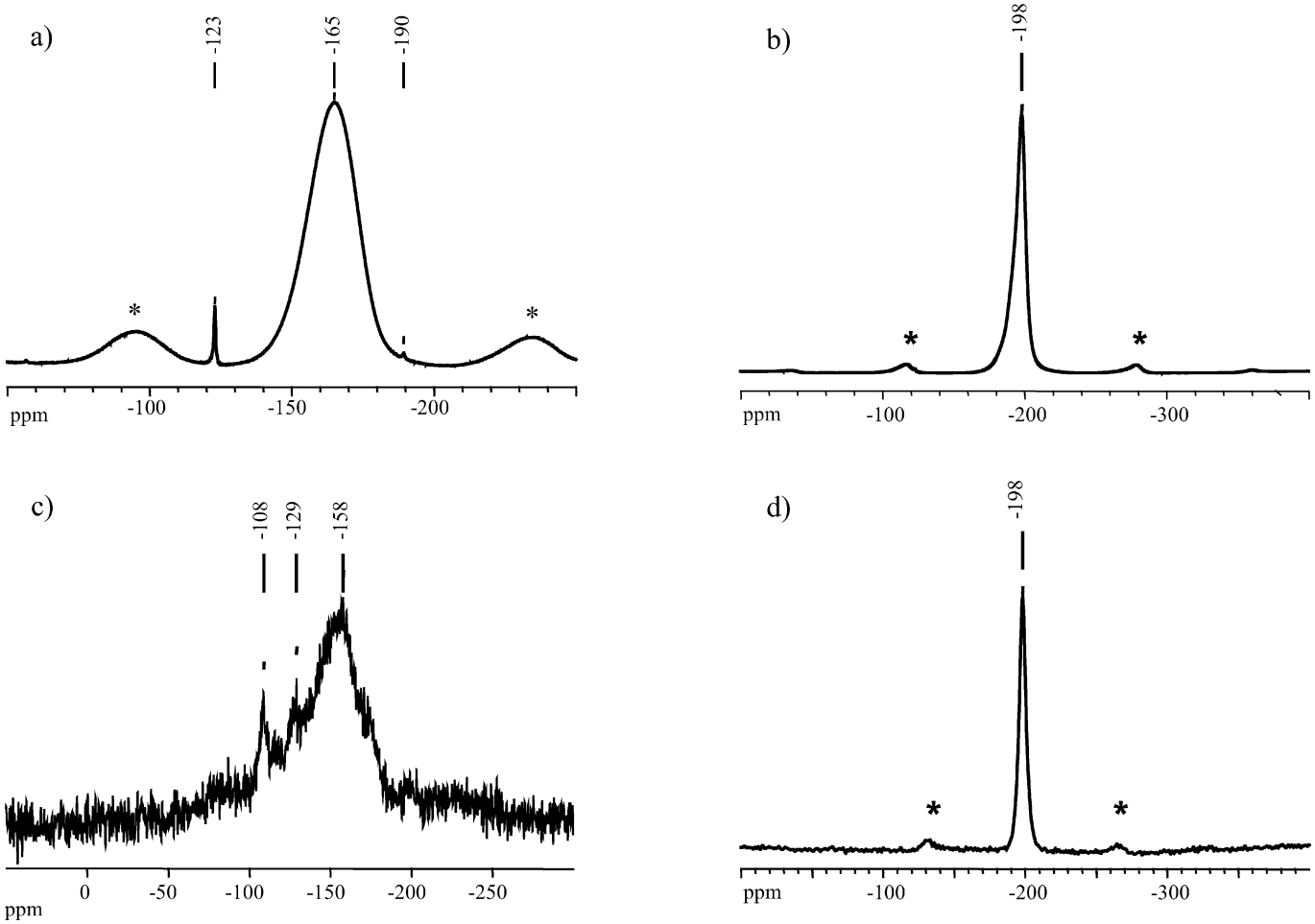

Fig. 2: ^{19}F MAS NMR spectra (central signals) of (a) AlF_3 and (b) MgF_2 after drying at 180 °C as well as (c) AlF_3 and (d) MgF_2 after thermal annealing at 900 °C in air (heating rate 20 °C/min, 4 h dwell time). Measurements were performed at spinning speeds of 25 kHz (a-c) or 20 kHz (d), respectively (*: spinning sidebands).

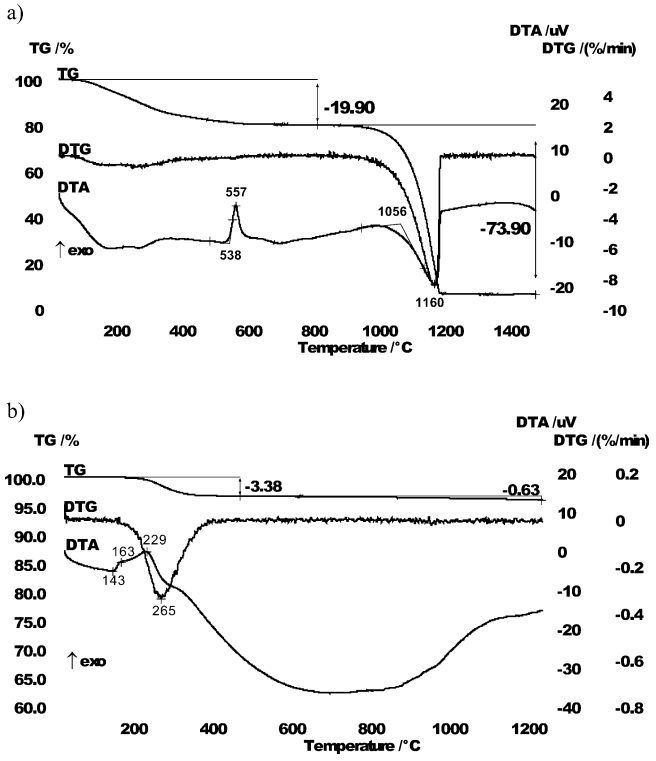

Fig. 3: Thermoanalytic plots of (a) AlF_3 and (b) MgF_2.

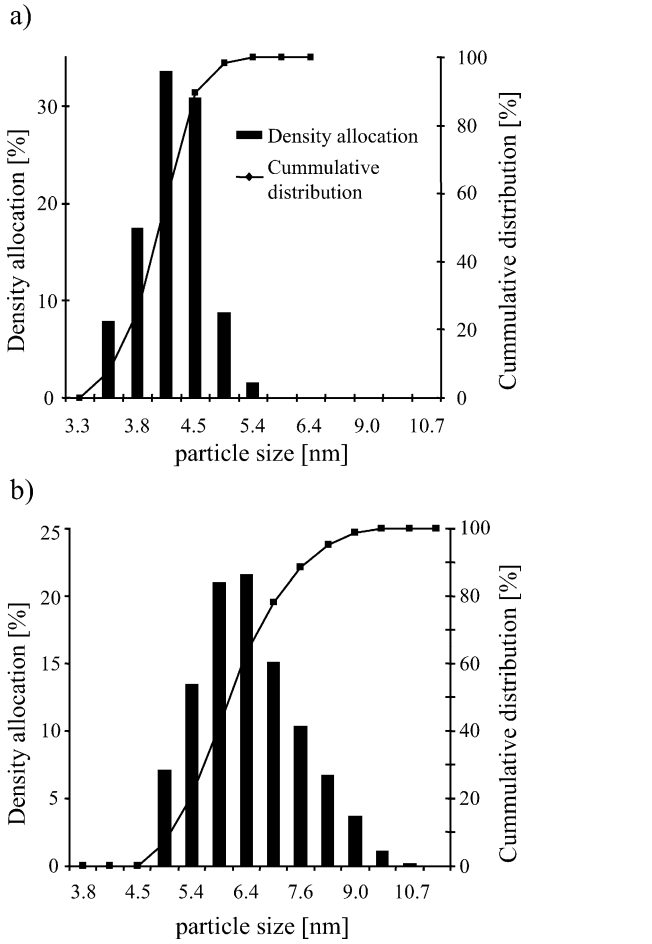

Fig. 4: Particle size distribution of pure fluoride phases (a) AlF_3 (d_{16} = 3.6 nm, d_{50} = 4.1 nm; d_{95} = 4.7 nm) and (b) MgF_2 (d_{16} = 5.2 nm, d_{50} = 6.1 nm; d_{95} = 8.3 nm).

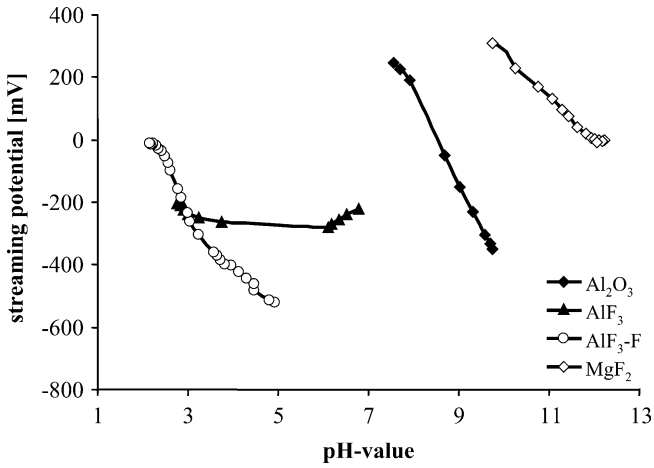

Fig. 5: Electrochemical streaming potentials of nanoscopic fluorides in comparison with pure alumina. Isoelectric points: Al_2O_3: pH_{iso}= 8.5; AlF_3: pH_{iso}< 2; AlF_3-F: pH_{iso}< 2; MgF_2: pH_{iso}= 12.2; AlF_3-F: post-fluorinated AlF_3.

(2) Synthesis, characterization and thermal behaviour of the ceramic samples

The ceramic samples were produced according to the procedure described above. In Fig. 6, SEM images of polished and thermally etched probes of calcined and finally HIP-processed alumina ceramics doped with 0.1 wt% MgO and MgF_2, respectively, are shown. The densities of these samples correspond to theoretical density. As can be seen, MgF_2 doped samples (Fig. 6, a) are built up by smaller particles with a far more homogeneous sub-micron structure as compared to the state-of-the-art MgO-doped sample (Fig. 6, b).

For the polished and thermally etched probes after HIP processing, the following structural characteristics were obtained: mean particle (crystallite) size: d_{50} = 0.35 µm; surface roughness (polished): R_a < 6 nm; Vickers hardness: HV0,1 = 3200 and inline transmission at λ = 780 nm: > 65%. For comparison, the standard characteristics for MgO-doped samples are given: mean particle (crystallite) size: d_{50} ≈ 0.60 µm; surface roughness (polished): R_a < 15 nm; Vickers hardness: HV0,1 = 2200 and inline transmission at λ = 780 nm: > 61 %. Thus, as a result of the addition of MgF_2 instead of MgO, significantly improved homogeneity and a narrower particle size distribution was obtained (cf. Fig. 6a and 6b), resulting in a more or less defect-free structure with positive effects for the surface roughness and hardness.

Fig. 7 shows the transmission data obtained for MgO- and MgF_2-doped Al_2O_3 ceramic samples.

IV. Discussion

By employing the selected technology of powder dispersion and slip casting in combination with MgF_2-doping, it has proved possible to obtain alumina ceramics with a nearly defect-free as well as ultra-fine homogeneous structure. The average crystallite size of the finally calcined ce-

ramic was much smaller than 500 nm, and hence, superior to samples that were conventionally prepared on the basis of MgO. As a result, almost transparent and extremely hard (Vickers hardness of about 3200 compared to only 2200 for MgO as additive) ceramic samples were manufactured, which is doubtless a result of the action of nano-metal fluoride doping. However, the action of the both nanoscopic metal fluorides (MgF_2 and AlF_3) investigated here is contrarily different. On first glance, one might assume the main reason for this arises from the very different zeta-potentials of both materials resulting in different stabilities of the slurries. That is, preparing a slurry at pH = 7 with AlF_3 might result in coagulation because the surface charge of Al_2O_3 is positive but for AlF_3 it is negative. In contrast, with MgF_2 the situation is different, both potentials are positive thus repulsive forces will occur, stabilising the slurry. However, there is strong evidence that – in contrast to this expectation – MgF_2 from sols is immediately spread over the Al_2O_3-grains as will be shown later. And it is especially this effect which makes nano-MgF_2 so effective as a sintering agent. Since the main effect for the drastically improved ceramic properties originates from the nanoscopic nature of the fluorides, the big difference between AlF_3 on one hand and MgF_2 on the other results from the different thermal behaviour of the two metal fluorides, as will be discussed in more detail in the following.

(1) Aluminium fluoride as dopant

Although AlF_3 is reported in the literature as a good candidate to be used as an additive for reducing the calcination temperature in ceramic manufacturing [29, 30], our results cannot at all re-confirm the suitability of AlF_3. That is, AlF_3, and especially nanoscopic AlF_3, on one hand shows a strong tendency toward sublimation, obviously because of a significant covalency character in this compound. Thus, as evidenced by MS-coupled DTA-TG-measurements, AlF_3 starts to sublime (to a very low extent) already at around 700 °C, thus causing blowing of the ceramic samples, resulting in final products with unacceptably high porosity and low density. However, even more critical is the strong tendency of AlF_3 towards pyrohydrolysis. As has been shown in [15, 16], AlF_3 can fully be hydrolyzed in the course of heating up until 700 °C in presence of a moist gas atmosphere or if water (adsorbed or as structural water) is already present in the starting material. Thus, under real technical conditions of ceramic manufacturing, during calcination either sublimation of AlF_3, starting at around 700 °C, or hydrolysis, causing HF-elimination, will contradict the targeted aim, namely obtaining denser solids.

(2) MgF_2 as additive

The situation is totally different in the case of MgF_2. This material, even nanoscopic MgF_2, is almost resistant to pyrohydrolysis. The DTA-TG-investigations do not show any changes until 1250 °C and even with the coupled, very sensitive mass spectrometry just traces of evolving species can be detected. Even in the presence of a moist gas phase, MgF_2 exhibits a surprisingly high hydrolysis resistance. Thus, after removal of weakly adsorbed water, MgF_2 shows almost no hydrolysis up to 1250 °C, thus ensuring perfect thermal properties for use as a sintering additive.

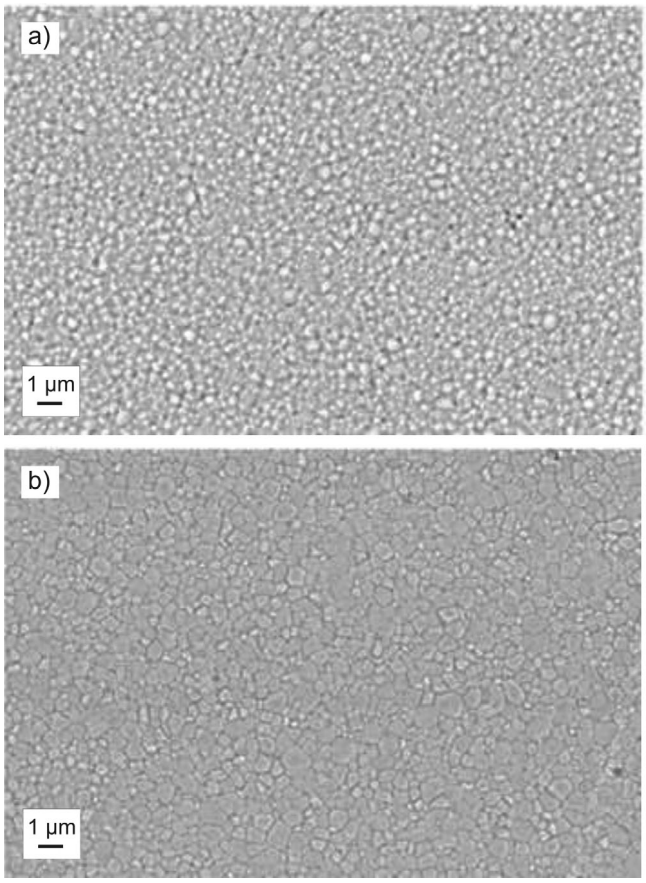

Fig. 6: SEM images (10 000 times magnified) of (a) MgF_2-doped and (b) MgO-doped alumina ceramics after HIP processing.

(3) The supposed mechanism

Although the available experimental results do not permit definite conclusions to be drawn regarding the action of the MgF_2, there is some experimental evidence especially arising from ^{19}F MAS NMR to speculate about the mechanism. The ^{19}F MAS NMR spectra of mixtures of MgF_2 and corundum powder in absence and presence of some water (afterwards dried at about 100 °C) clearly show that the intensity of the ^{19}F-peak, characteristic for F bonded in MgF_2, diminished significantly for the sample that was previously wetted. At the same time, a clear signal in the region of -150 ppm becomes visible, being a definite indication of F bonded to surface aluminium sites [31]. However, it is impossible that below 100 °C a kind of solid state reaction between MgF_2 and Al_2O_3 has thus formed "real" Al-F-phases. This is indirectly but strongly supported by the fact that MgF_2-doped ceramic samples do not at all show the blowing effect that was observed with pure AlF_3 as additive. Hence, it seems that the small nano-MgF_2 particles become extremely finely

spread over the surface of the corundum crystallites, thus providing ideal conditions for sintering. It might be speculated that such nanoscopic thin MgF_2 form micro- (better nano-) melts during sintering, thus reducing the necessary final sintering temperature and drastically increasing the binding force between the corundum crystallites. On this basis, the observed transparency as well as hardness of the final MgF_2-doped corundum ceramics may be rationalized this way.

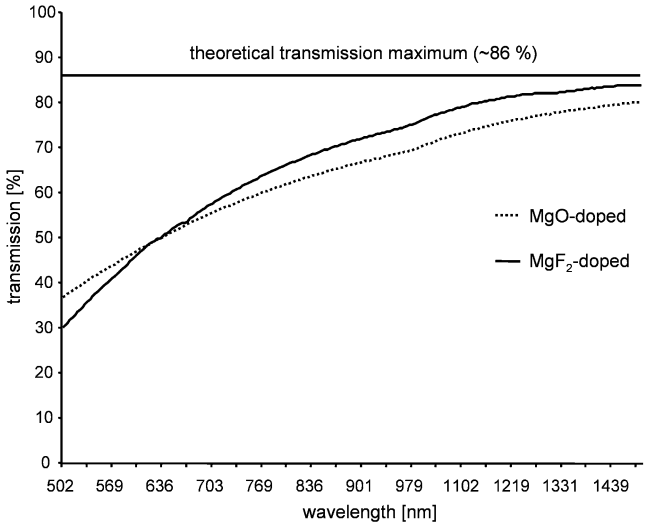

Fig. 7: Transmission measurements of transparent MgF_2-doped and MgO-doped alumina ceramics.

Finally, it is worth noting that neither classically prepared AlF_3 nor MgF_2 exhibited similar effects. In all these cases where powdered but crystalline materials were used, the quality of the sintered ceramic in all the properties (density, transparency and hardness) was significantly worse.

V. Conclusion

In conclusion, the results presented here clearly show that addition of nanoscopic magnesium fluoride enables effective limitation of grain growth when compared to the standard ceramic production. Nanoscopic MgF_2 is superior to conventionally used MgO. Not only the final sintering temperature is reduced but even more importantly as a result of this, the grain size of the final ceramic material is drastically below 500 nm, resulting in an unexpected high Vickers hardness of 3200 combined with an excellent inline transmission above 65 %. Thus, with the new sintering material, nano-MgF_2, exciting properties for Al_2O_3 ceramics can be achieved, opening up new applications for this improved material.

In contrast, nano-AlF_3 is not suitable for the preparation of slurries and spray granulates with application of the standard technology mainly owing to

i) its extreme *Lewis*-acidity,
ii) phase transformation and sublimation starting at around 700 °C, and
iii) its strong tendency toward pyrohydrolysis resulting overall in outgassing effects, which ultimately prevent the use of nano-AlF_3 powders for technical applications.

With the use of nano-MgF_2, it is possible to obtain ceramics with high density, sub-µm grain size and low defect concentrations, which are preconditions for an improvement of mechanical strength, transparency as well as optical properties.

The application of nanoscopic MgF_2 provides the best homogeneity and smallest grain size in the final ceramic material and thus opens up a new approach to a technologically profitable and economic preparation process of corundum ceramics with enhanced properties.

Last not least, the possible chemical role of nano-MgF_2 in the course of texture formation, crystal growth, and densification of the corundum particles can be at least partly rationalized based on DTA-TG and ^{19}F MAS NMR-investigations.

Acknowledgements

The assistance of Dr M. Feist (Humboldt University of Berlin, Department of Chemistry), who conducted the thermoanalytical measurements, is gratefully acknowledged.

References

1 Ismagilov, Z.R., Shkrabina, R.A., Koryabkina, N.A., Kirchanov, A.A., Veringa, H., Pex, P.: Porous alumina as a support for catalysts and membranes. Preparation and study, *React. Kinet. Catal. Lett.*, **60**, 225-231, (1997).

2 Kwon, S., Messing, G.L.: Constrained densification in boehmite alumina mixtures for the fabrication of porous alumina ceramics, *J. Mater. Sci.*, **33**, 913-921, (1998).

3 Apetz, R., van Bruggen, M.P.B.: Transparent alumina: A light-scattering model, *J. Am. Ceram. Soc.*, **86**, 480-486, (2003).

4 Krell, A., Hutzler, T., Klimke, J.: Transparent ceramics for structural applications: Part 2: Fields of applications, *Cfi-Ceram. Forum Int.*, **84**, E50-E56, (2007).

5 Krell, A., Ma, H.W.: Sintering transparent and other sub-µm alumina: The right powder, *Cfi - Ceram. Forum Int.*, **80**, E41-E45, (2003).

6 Skrovanek, S.D., Bradt, R.C.: Microhardness of a Fine-Grain-Size Al_2O_3, *J. Am. Ceram. Soc.*, **62**, 215-216, (1979).

7 Berry, K.A., Harmer, M.P.: Effect of MgO Solute on Microstructure Development in Al_2O_3, *J. Am. Ceram. Soc.*, **69**, 143-149, (1986).

8 Yokota, K.: Influence of Mg^{2+} ions Adsorption onto Alpha-Alumina Particle Surfaces on Forming and Sintering Properties in Alumina Compacts, In: 10th ECerS Conf., Berlin, (2007).

9 Belov, S.F., Rosdin, I.A., Plisko, W.N., Buschujev, J.G.: *Neorg. Mat.*, **16**, 1026-1028, (1980).

10 Krell, A., Klimke, J.: Effects of the homogeneity of particle coordination on solid-state sintering of transparent alumina, *J. Am. Ceram. Soc.*, **89**, 1985-1992, (2006).

11 Scholz, G., Dörfel, I., Heidemann, D., Feist, M., Stösser, R.: Nanocrystalline CaF_2 particles obtained by high-energy ball milling, *J. Solid State Chem.*, **179**, 1119-1128, (2006).

12 Scholz, G., König, R., Petersen, J., Angelow, B., Dorfel, I., Kemnitz, E.: Mechanical Activation of alpha-AlF_3: Changes in Structure and Reactivity, *Chem. Mater.*, **20**, 5406-5413, (2008).

13 Kemnitz, E., Gross, U., Rüdiger, S., Shekar, S.C.: Amorphous Metal Fluorides with Extraordinary High Surface Areas, *Angew. Chem. Int. Ed.*, **42**, 4251-4254, (2003).

14 Kemnitz, E., Gross, U., Rüdiger, S., Shekar, S.C.: Amorphous Metal Fluorides with Extraordinarily High Specific Surface Areas (in German), *Angew. Chem.*, **115**, 4383-4386, (2003).

15 Stosiek, Ch., Brehme, S., Scholz, G., Kemnitz, E.: Influence of milling, sonication and fluoride doping of pseudoboehmites on their phase transformation behaviour to corundum, *J. Eur. Ceram. Soc.*, **29**, 2713-2720, (2009).

16 Stosiek, Ch., Scholz, G., Eltanany, G., Bertram, R., Kemnitz, E.: Novel synthesis and thermal behaviour of aluminium hydroxy fluorides $AlF_x(OH)_{3-x}$, *Chem. Mater.*, 20, 5687-5697, (2008).

17 JCPDS-ICDD – International Centre for Diffraction Data: *PDF-2 Database (Sets 1-51 plus 70-89)*. PA 19073-3273 U.S.A., Release 2001. - PCPDFWIN Version 2.2.

18 Cory, D.G., Ritchey, W.M.: Suppression of signals from the probe in Bloch decay spectra, *J. Magn. Reson.*, **80**, 128-132, (1988).

19 Rüdiger, S.K., Gross, U., Feist, M., Prescott, H.A., Shekar, S.C., Troyanov, S.I., Kemnitz, E.: Non-aqueous synthesis of high surface area aluminium fluoride - a mechanistic investigation, *J. Mater. Chem.*, **15**, 588-597, (2005).

20 Wuttke, S., Coman, S.M., Scholz, G., Kirmse, H., Vimont, A., Daturi, M., Schroeder, S.L.M., Kemnitz, E.: Novel Sol-Gel Synthesis of Acidic $MgF_{2-x}(OH)_x$ Materials, *Chem. Eur. J.*, **14**, 11488-11499, (2008).

21 König, R., Scholz, G., Bertram, R., Kemnitz, E.: Crystalline aluminium hydroxy fluorides – suitable reference compounds for ^{19}F chemical shift trend analysis of related amorphous solids, *J. Fluorine Chem.*, **129**, 598-606, 2008.

22 König, R., Scholz, G., Pawlik, A., Jäger, C., van Rossum, B., Oschkinat, H., Kemnitz, E.: Crystalline Aluminum Hydroxy Fluorides: Structural Insights Obtained by High Field Solid State NMR and Trend Analyses, *J. Phys. Chem. C*, **112**, 15708-15720, (2008).

23 Delmotte, L., Soulard, M., Guth, F., Seive, A., Lopez, A., Guth, J.L.: ^{19}F MAS NMR studies of crystalline microporous solids synthesized in the fluoride medium, *Zeolites*, **10**, 778-783, (1990).

24 Guth, J.L., Delmotte, L., Soulard, M., Brunard, N., Joly, J.F., Espinat, D.: Synthesis of Al, Si-MFI-type zeolites in the presence of fluoride anions: structural and physicochemical characteristics, *Zeolites*, **12**, 929-935, (1992).

25 Krahl, T., Stösser, R., Kemnitz, E., Scholz, G., Feist, M., Silly, G., Buzare, J.-Y.: Structural Insights into Aluminum Chlorofluoride (ACF), *Inorg. Chem.*, **42**, 6474-6483, (2003).

26 Scholz, G., Korup, O.: High-energy ball milling – a possible synthesis route for cryolite and chiolite, *Solid State Sci.*, **8**, 678-684, (2006).

27 Prescott, H. A., Li, Z.-J., Kemnitz, E., Deutsch, J., Lieske, H.: New magnesium oxide fluorides with hydroxy groups as catalysts for Michael additions, *J. Mater. Chem.*, **15**, 4616-4628, (2005).

28 Menz, D., Mensing, Ch., Hönle, W., von Schnering, H. G.: Thermal behaviour of aluminium fluoride hydroxide hydrate $AlF_{2,3}(OH)_{0,7}(H_2O)$ (in German), *Z. anorg. allg. Chem.*, **611**, 107-113, (1992).

29 Wu, Y., Zhang, Y., Pezzotti, G., Guo, J.: Influence of AlF_3 and ZnF_2 on the phase transformation of gamma to alpha alumina, *Mater. Lett.*, **52**, 366-369, (2002).

30 Zivkovic, Z., Strbac, N., Sestak, J.: Influence of fluorides on polymorphous transformation of α-Al_2O_3 formation, *Thermochim. Acta*, **266**, 293-300, (1995).

31 Nordin, J.P., Sullivan, D.J., Phillips, B.L., Casey, W.H.: Mechanisms for fluoride-promoted dissolution of bayerite [β-$Al(OH)_3$(s)] and boehmite [γ-AlOOH]: ^{19}F-NMR spectroscopy and aqueous surface chemistry, *Geochim. Cosmochim. Acta*, **63**, 3513-3524, (1999).